Interplay between mucus mobility and alveolar macrophage targeting of surface-modified liposomes

Kamila Bohne Japiassu, Francois Fay, Alessandro Marengo, Younès Louaguenouni, Catherine Cailleau, Stéphanie Denis, David Chapron, Nicolas Tsapis, Thais Leite Nascimento, Eliana Martins Lima, et al.

Interplay between mucus mobility and alveolar macrophage targeting of surface-modified liposomes

Kamila Bohne Japiassu[a,b], Francois Fay[a], Alessandro Marengo[a], Younès Louaguenouni[a], Catherine Cailleau[a], Stéphanie Denis[a], David Chapron[a], Nicolas Tsapis[a], Thais Leite Nascimento[b], Eliana Martins Lima[b] and Elias Fattal[a*]

a)Université Paris-Saclay, CNRS, Institut Galien Paris-Saclay 91400, Orsay, France. *e-mail: elias.fattal@universite-paris-saclay.fr

b)Center for RD&I in Pharmaceutical Nano/Technology (FarmaTec), Federal University of Goias, Goiania, 74605-220 Goias, Brazil.

Abstract

Alveolar macrophages play a crucial role in the initiation and resolution of the immune response in the lungs. Pro-inflammatory M1 alveolar macrophages are an interesting target for treating inflammatory and infectious pulmonary diseases. One commune targeting strategy is to use nanoparticles conjugated with hyaluronic acid, which interact with CD44 overexpressed on the membrane of those cells. Unfortunately, this coating strategy may be countered by the presence on the surface of the nanoparticles of a poly(ethylene glycol) corona employed to improve nanoparticles' diffusion in the lung mucus. This study aims to measure this phenomenon by comparing the behavior in a murine lung inflammation model of three liposomal platforms designed to represent different poly(ethylene glycol) and hyaluronic acid densities (Liposome-PEG, Liposome-PEG-HA and Liposome-HA). In this work, the liposomes were obtained by one-step ethanol injection method. Their interaction with mucin and targeting ability toward pro-inflammatory macrophages were then investigated *in vitro* and *in vivo* in a LPS model of lung inflammation. *In vitro*, poly(ethylene glycol) free HA-liposomes display a superior targeting efficiency toward M1 macrophages, while the addition of poly(ethylene glycol) induces better mucus mobility. Interestingly *in vivo* studies revealed that the three liposomes showed distinct cell specificity with alveolar macrophages demonstrating an avidity for poly(ethylene glycol) free HA-liposomes, while neutrophils favored PEGylated liposomes exempt of HA. Those results could be explained by the presence of two forces exercising a balance between mucus penetration and receptor targeting. This study corroborates the importance of considering the site of action and the targeted cells when designing nanoparticles to treat lung diseases.

Keywords: *Liposome, Hyaluronic acid, Poly(ethylene glycol), M1 macrophages, CD44, Lung injury.*

1. Introduction

In order to protect the lung tissue and the body against inhaled particles and microorganisms, the respiratory system possesses several mechanical and immunological defense strategies [1,2]. Mechanical protections include the progressive segmentation of the airway structure, the mucociliary clearance by ciliated epithelial cells, and the presence of a glycoprotein-based mucus layer on the airway surfaces [3]. This mucus layer is mainly composed of mucin and covers the entire respiratory epithelium, forming a protective physical barrier against pathogens as well as therapeutic molecules and delivering agents [4,5]. The protective action of the mucus is supported by the phagocytic activity of neutrophils and macrophages, including alveolar macrophages. Those macrophages are specifically located in the mucus covering the epithelial layer and the alveoli tissues [1]. Alveolar macrophages also present significant functional and phenotypical specialization, allowing active responses to environmental signals and pathogens through rapid phenotype alterations [6,7], such as polarization toward a classically activated (M1) state.

Macrophage polarization in a M1 phenotype is an essential property that helps eliminate foreign materials and pathogens from the lungs [8]. M1 macrophages exhibit a pro-inflammatory profile and are characterized by the production of high levels of pro-inflammatory cytokines and increased expression of CD44 [9]. M1 macrophages are known to mediate resistance toward intracellular parasites (*i.e*., bacteria, protozoa, and viruses) and antitumor immunity [10]. Evidences have shown that an imbalanced macrophage polarization can have adverse effects, resulting in inflammatory diseases, including COPD [11]. In addition, they are present in more significant amounts in diseases such as tuberculosis, severe acute respiratory syndrome (SARS) and pulmonary hypertension [9]. Therefore, M1 activated alveolar macrophages are attractive cell targets for treating inflammatory and infectious pulmonary diseases [12].

The development of nanoparticles for lung administration and cell-specific delivery has historically faced the need to optimize particles physical characteristics based on conflicting requirements. One well-studied prerequisite,

is the size of the particles. Indeed, large nanoparticles (> 1 µm) have demonstrated better alveoli accumulation after nebulization, while small particles (< 260 nm) tend to be preferentially internalized by cells [13]. Another critical feature investigated in pulmonary delivery has been the interactions between nanoparticles and mucus, which acts as a critical barrier. Thus, the deposited nanoparticles must either dissolve or cross the mucus layer to avoid mucociliary clearance and exert their therapeutic activity [14]. Several studies have demonstrated that the addition of a poly(ethylene glycol) (PEG) coating layer at the surface of nanoparticles significantly increases their diffusion in mucus [15,16]. This strategy has been successfully applied to the pulmonary delivery of nanoparticles containing corticosteroids, with PEGylated nanoparticles showing superior activity compared to non-mucopenetrating ones [18,19].

Another common surface modification is the conjugation of targeting moieties *i.e.* sugars, peptides, proteins, or aptamers to actively target receptors overexpressed on specific cells such as cancer, endothelial or immune cells [20,21]. In the last decade, several teams, including our laboratory, have developed an array of surface coating strategies to target the CD44 receptor that is overexpressed by several key cell types, including cancer stem cells and activated pro-inflammatory M1 macrophages [21–23]. Successful anti-CD44 ligands include antibodies [24], aptamers [23] as well as hyaluronic acids (HA) [25], which is the natural ligand of the CD44 receptor.

Unfortunately, when applied simultaneously, PEGylation and ligand conjugation strategies may have a detrimental effect on each other. Indeed, the presence of targeting moieties on nanoparticle surface may compromise the pharmacokinetic characteristics of the PEGylated nanoparticles [26] or their mucopenetration [16]. Similarly, an excess of PEG polymers may sterically shield the ligands, preventing their interaction with the targeted receptors and thus limiting the particle receptor-specific cellular uptake [27].

This study was designed to evaluate three lipid platforms representing various levels of PEGylation and active targeting, using HA as a model ligand. Using an array of physical and biological assays, the three platforms were compared with one another to explore how their surface physicochemical

characteristics dictate their mucopenetrating ability and their capacity to target cells both *in vitro* and *in vivo*.

2. Materials and Methods

2.1. Materials

Phospholipids 1,2-dihexadecanoyl-sn-glycero-3-phosphocholine (DPPC), 1,2-dipalmitoyl-snglycero-3-phosphoethanolamine (DPPE) and 1,2-distearoyl-sn-glycero-3-phosphoethanolamine-N-[methoxy(polyethylene-glycol)-2000] (ammonium salt) were purchased from Lipoid Gmbh (Germany). L-α-phosphatidylethanolamine-N-(lissamine rhodamine B sulfonyl) (PE-Rhodamine) and PE-fluorescein were purchased from Avanti Polar Lipids (USA). Cholesterol (CHOL), ethyl(dimethylaminopropyl) carbodiimide (EDC), N-Hydroxysuccinimide (NHS), *t*-butanol, lipopolysaccharides from *Escherichia coli* O127:B8 (LPS), collagenase type IV, DNAse I, and mucin type III were obtained from Sigma-Aldrich (France). Hyaluronic acid (400 kDa) was purchased from Contipro (Czech Republic). Recombinant murine IL-4, recombinant murine IL-13 and recombinant murine IFN-γ were obtained from PeproTech (France). MilliQ® water was obtained using a MilliQ® reference system from Merck-Millipore. Solvents were of HPLC analytical grade and were obtained from Carlo Erba (Italy). The following monoclonal antibodies were purchased from Thermo Fisher (USA): Anti-Mo F4/80 (clone BM8); anti-Ly-6G (clone 1A8); anti-CD170/Siglec-F (clone 1RNM44N); anti-CD11b (clone M1/70); anti-Arginase 1 (clone A1exF5); Anti-iNOS (clone CXNF); anti-CD206/MMR (clone MR6F3), and anti-CD86 (clone B7-2) monoclonal antibody (clone GL1) 12-0862-81. Antibody Anti-Mo CD44 (clone IM7) and anti-mouse CD16/CD32 (clone 2.4G2, Mouse BD Fc Block™) were obtained from BD Biosciences (USA). TNF-alpha Mouse Uncoated ELISA Kit was purchased from Thermo Fisher (USA).

2.2. Liposome preparation

400 kDa HAs were conjugated to DPPE molecules through EDC/NHS chemistry using a protocol developed in a previous study [28]. The three liposomal formulations were prepared as follow. PEGylated liposomes (Lip-PEG) were composed of DPPC, CHOL and mPEG-DSPE in a 65:30:5 molar ratio and a total amount of 40 mg of lipids per batch (Table 1). Liposomes were

prepared by the ethanol injection method [29]. Phospholipids and CHOL were dissolved in absolute ethanol and heated at 43 °C for 10 min. One mL of the organic phase was injected at 1.3 mL/min into 10 mL of MilliQ® water under stirring (900 rpm) using an automatic injector. The resulting suspension was stirred for 15 min, and the mixture of ethanol was removed under vacuum using a rotary evaporator. The liposomal suspension was then ultracentrifuged for 4 h at 72,500 x g and 4 °C. The supernatant was discarded, and the liposomes were resuspended in 10 mL of MilliQ® water. Finally, the liposomal suspension was centrifuged at 1,700 x g for 30 min to eliminate large aggregates. As showed in table 1, hyaluronic acid decorated PEGylated liposomes (Lip-PEG-HA) were prepared by replacing part of the mPEG-DSPE with HA-DPPE conjugate while Hyaluronic acid decorated liposomes (Lip-HA) were prepared by replacing the total amount of mPEG-DSPE with HA-DPPE conjugate and then, the lipids were solubilized in *t*-butanol/water mixture (60:40).

Fluorescent liposomes were prepared by adding 1% w/w of PE-Rhodamine or PE-fluorescein to liposome composition.

Table 1: Lip-PEG, Lip-PEG-HA and Lip-HA lipid composition for 10 mL of the formulation.

Compounds (µMol)	**Lip-PEG**	**Lip-PEG-HA**	**Lip-HA**
DPPC	35	35	35
CHOL	16.5	16.5	16.5
mPEG-DSPE	3.8	1.8	-
HA-DPPE	-	0.01	0.019

2.3. Liposome characterization

Liposome sizes, polydispersity indexes (PdI) and zeta (ζ) potentials were analyzed by dynamic light scattering (DLS) using a Nano ZS (Malvern instruments, UK). Liposomal suspensions were diluted by a factor 10 either in MilliQ® water for size measurements, or in 1 mM NaCl for ζ potential measurements. DLS measurements were done in triplicates of 10 consecutive runs. DPPC concentrations were determined by an enzymatic colorimetric method following the manufacturer's instructions (Biolabo, France). Loss of other lipids was considered proportional to the loss of DPPC. The interaction between HA-DPPE and DPPC bilayer was evaluated by differential scanning calorimetry (DSC) using a microcal VP-DSC (MicroCal). DSC analyses were performed from 25 to 60 °C at a heating rate of 1.5 °C/min.

The rhodamine encapsulation rate was quantified by spectroscopy by solubilizing and diluting the various lipids forming the liposomes in an ethanol solution. The absorbance of the resulting solutions was measured at 560 nm (absorption peak of rhodamine). The encapsulation rate was calculated using a calibration curve obtained by diluting a solution of PE-Rhodamine in the range of 1 to 10 µg/mL.

2.4. Cell culture

Murine macrophage cell line RAW 264.7 (ATTC TIB-71), obtained from ATCC were grown in Dulbecco's modified Eagle's medium supplemented with 10% fetal bovine serum, 50 U/mL penicillin and 50 U/mL streptomycin, in a humidified incubator at 37 °C supplied with 5% CO_2. Cells were split twice per week at a 1/10 ratio using a scraper and were used between passages 4 to14 after thawing.

2.5. Macrophage polarization

RAW 264.7 macrophages were seeded onto 12-well culture plates at 3 × 10^5 cells per 1 mL of culture medium and cultured for 24 h. For M1 polarization, macrophages were pretreated with interferon-γ (IFN-γ) and lipopolysaccharide (LPS). Cell polarization was evaluated by mRNA expression of NOS2 (5'→3' GAGACAGGGAAGTCTGAAGCAC; 3'→5'

CCAGCAGTAGTTGCTCCTCTTC) and TNF-α (5'→3' GGTGCCTATGTCTCAGCCTCTT; 3'→5' GCCATAGAACTGATGAGAGGGAG) by real-time quantitative PCR (qPCR). mRNAs were extracted using a RNeasy kit and reverse-transcribed into cDNA using the QuantiTect reverse transcription kit both from Qiagen (France) according to the manufacturer's instructions. qPCR measures were obtained using a Power SYBR green kit (Life Technologies, Inc., USA) and a Mx3000P system (Stratagene, USA) according to the manufacturers' instructions. PCR cycle was set as follows: 95 °C for 15 s, 60 °C for 30 s, and then 72 °C for 30 s for 40 cycles. Gene expression values were standardized using the basal GAPDH expression and compared to untreated cells. Expression of CD86, iNOS, CCR-2, Arg-1 and CD-44 was evaluated via flow cytometry using primary antibodies (Thermo Fisher Scientific, USA). After polarization, cells were incubated with mouse BD Fc Block™ and then incubated, for 30 min at 4 °C, with antibodies targeting CD86, CD44 or iNOS according to manufacturer instructions. For iNOS staining, a 10-minute permeabilization step with a solution of 0.1% saponin was carried out before antibody incubation. After incubation, cells were washed three times with 1 mL of FACS buffer, centrifuged at 400 x g for 5 min at 4 °C, and resuspended in 800 µL of FACS buffer. Cell fluorescence was acquired using a BD Accuri C6 Cytometer (BD Biosciences, USA) and the data were analyzed using CFlow Plus software (BD Biosciences, USA).

2.6. *In vitro* liposomes uptake

RAW 264.7 macrophages were polarized into M1 phenotype by treating them with IFN-γ (50 ng/mL), followed at 6h by the addition of 100 ng/mL of lipopolysaccharide (LPS)and a total 24 h of incubation. The medium was then replaced by a fresh medium and the cells were incubated with PE-Rhodamine labeled Lip-PEG, Lip-PEG-HA and Lip-HA normalized on the rhodamine content. After incubation, the cells were washed twice with FACS buffer, collected using a cell scraper and resuspended in 1 mL of FACS buffer. Cell-liposomes interactions were measured using a BD Accuri C6 Cytometer (BD Biosciences, USA) and the data were analyzed using CFlow Plus software (BD Biosciences, USA) using cells incubated in the absence of liposomes as control.

2.7. Confocal Microscopy

Liposome uptake was evaluated qualitatively by using confocal microscopy. RAW 264.7 cells were seeded in IBIDI 8-chamber polystyrene vessels (50.000 cells/well) and grown overnight at 37 °C and 5% CO_2 in a culture medium. After 24 h macrophages were polarized into M1 phenotype as described in 2.6. The cells were then treated with different rhodamine-labelled liposomes at the final rhodamine concentration of 0.8 µM. After 6 h incubation cells were washed with PBS, fixed using 4% (v/v) paraformaldehyde and embedded in mountain medium with DAPI.

Fluorescence images were performed with an inverted STED-gated Leica TCS SP8 microscope (Leica, Germany) using a 63×/1.4 HC PL APO CS2 oil immersion objective lens and white light laser. Red fluorescence emission was collected with a 565–620 nm wide emission slit using a sequential mode. The pinhole was set at 1.0 Airy unit (0.8 µm optical slice thickness). Images were acquired with the Leica SP8 LAS X software (Version 2.0.1; Leica, Germany).

2.8. Multiple particle tracking

20 µL of liposome formulations were diluted in 180 µL of 2 mg/mL mucin solution previously filtered to eliminate large aggregates. Ten-second movies at 66.7 ms temporal resolution were acquired at 37 °C using Zeiss video microscope. Movies were analyzed with Imaris software (Oxford Instruments). The mean square displacements (MSD) of at least ten particles per formulation were analyzed as a function of time.

2.9. Lung inflammation model

In vivo experimental procedures using C57BL/6J mice were approved by the C2EA – 26J Ethics Committee in Animal Experimentation of IRCIV, under the protocol APAFIS#27142-2020091114373465. Experiments were conducted following the European guidelines (86/609/EEC and 2010/63/EU) and the Principles of Laboratory Animal Care and national French regulations on animal testing (Decree No. 2013−118 of February 1, 2013). C57BL/6J male mice aged 7–12 weeks-old (Janvier Labs, France) were acclimated for at least one week before the experiments. Animals were kept under climate-controlled conditions with a 12 h light/dark cycle, constant temperature (19−22 °C), controlled relative humidity (45−65%), and food and water *ad libitum*.

The acute LPS-induced murine lung inflammation model was established in C57BL/6J mice following a protocol similar to Knapp *et al.* [30]. The mice were first anesthetized by intraperitoneal injection with a ketamine/xylazine mixture (100 and 10 mg/kg, respectively), and monitored until the disappearance of the pedal reflex. Using a 200 µL pipette, 15 µL of a LPS solution (2 mg/mL) was administered twice to the mice, by nasal administration (1.2 µL of LPS solution/g of mouse weight; *i.e.* 2.4 mg/kg). The mice were placed on their backs and the solution was injected through their nostrils. Subsequently, the mice were allowed to wake up and were monitored daily until euthanized.

At selected time points, animals were euthanized using an intraperitoneal overdose of pentobarbital (180 mg/kg). After the animal's death was confirmed, the trachea was exposed through an incision and cannulated with a 22-gauge catheter (BD Biosciences). Subsequently, bronchoalveolar lavage was performed 8 consecutive times by flushing the lungs with 0.7 mL (1 x 0.3 mL + 1 x 0.4 mL) plus 6 x 0.7 mL cold PBS to recover bronchoalveolar lavage fluid (BALF). The first two lavages were centrifuged at 400 x g for 10 min. The supernatant was kept for cytokine quantification by ELISA while the cellular pellets were pulled with the cells obtained from the subsequent lavages for flow cytometry analysis.

For flow cytometry, BALF cells were incubated with mouse BD Fc Block™ and then incubated, for 30 min at 4 °C, with antibodies targeting CD86, CD44 or iNOS according to manufacturer instructions. For iNOS staining, a 10-minute permeabilization step with a solution of 0.1% saponin was carried out before antibody incubation. After incubation, cells were washed with 2 mL of FACS buffer, centrifuged at 400 x g for 4 min at 4 °C, and resuspended in 200 µL of FACS buffer. Cell fluorescence was acquired using an Attune NxT® flow cytometer (Thermo Fisher Scientific, USA) and analyzed using FlowJo software (Tree Star, USA).

2.10. *In vivo* liposomes uptake

Acute LPS-induced lung inflammation was induced following the protocol described in 2.9. 24 h after LPS stimulation, mice were anesthetized. Rhodamine-labelled liposomes [Lip-PEG (*n=3*), Lip-PEG-HA (*n=4*) or Lip-HA (*n=3*)] were instilled into the mice lungs at a fixed rhodamine dose of 26 µg/kg

with the help of a mouse aerosolizer (Penn-Century, USA) [31]. Six hours after liposome instillation, animals were euthanized and BALF was recovered and processed as described in the previous section.

After BALF collection, animals were perfused with PBS. Lungs were then collected, diced and transferred to a 12-well plate with 2 mL of a collagenase IV 200 µg/mL + DNase I 10 µg/mL digestion solution in PBS for 40 min at 37 °C [32]. The reaction was stopped by adding 4 mL of FACS buffer. A single-cell suspension was made by removing tissue aggregates using cell strainers. Red blood cells were removed by lysis buffer. The cell pellets were resuspended in fresh FACS buffer.

BALF and lung cells were first stained for 30 min on ice with fixable viability dye eFluor™ 780 and then with monoclonal antibodies against F4/80, Ly-6G, Siglec F, and Cd11b for 30 min on ice according to the manufacturer instructions. Cells were then washed with 2 mL of FACS buffer, centrifuged at 400 x g for 4 min at 4°C, and resuspended in 200 µL of FACS buffer. Cell fluorescence was acquired using an Attune NxT® flow cytometer (Thermo Fisher Scientific, USA) and analyzed using FlowJo software (Tree Star, USA).

2.11. Statistical analysis

Results were reported as mean ± standard error of the mean (SD). Statistical differences between samples were evaluated using parametric t-test. All analyses were carried out with GraphPad Prism 6.0 statistical program (San Diego, USA). A p value < 0.05 was considered statistically significant (*).

3. Results and discussion

3.1. Preparation and characterization of liposomes

In this study, we compared the ability of 3 liposomal systems to target CD44-expressing M1 macrophages that are present in inflammatory lung diseases [2] choosing hyaluronic acid [34,35] with a high molecular weight as this ligand molecules has demonstrated a potent targeting efficiency toward immune cells [35,36]. Liposome surface can be easily decorated with hyaluronic acid by physical adsorption (electrostatic interactions) [37] or through the use of

phospholipids-HA conjugates [25]. To prevent loss of targeting HA within the mucus, the second strategy was chosen.

Hyaluronic acid-decorated liposomes (Lip-HA), untargeted PEGylated liposomes (Lip-PEG) and hyaluronic acid-decorated PEGylated liposomes (Lip-PEG-HA) (Figure 1A) were all prepared by a single step ethanol injection method [29] with a fixed amount of lipids (40 mg) while altering the ratio of the different lipid as indicated in Table 1. All liposomal platforms (Lip-HA, Lip-PEG and Lip-PEG-HA) demonstrated a homogeneous average particle diameter below 200 nm as indicated in Table 2. As expected, the presence of the large HA molecules on the surface of the liposomes led to an increase of their hydrodynamic diameters, as observed in other studies [23,35]. However, as demonstrated in later figures, this size increase did not lead to any detrimental effects on cellular uptake nor mucus mobility. The three liposomal preparations displayed a negative surface charge (ζ potential) without any significant differences between the formulations ($p > 0.05$). This negative charge was expected and desired to prevent charge interaction with the mucus, which is also negatively charged [38]. The introduction of mPEG-DSPE in the liposomal formulations also improved stability (Figure 1B). Indeed, while formations of clusters were observed in Lip-HA solutions after only one week at 4 °C, Lip-PEG and Lip-PEG-HA formulations were stable over 30 days without significant changes in size and PdI values.

Table 2: Characterization of liposomes. Average diameter (nm), PdI, ζ potential (mV) and rhodamine concentration (µM) of the three different liposome platforms Lip-PEG, Lip-PEG-HA and Lip-HA. Data are presented as average ± SD of *n=3* experiments.

Liposomes	**Average diameter (nm)**	**PdI**	**ζ potential (mV)**	**Rhodamine (µM)**
Lip-PEG	109 ± 5	0.16 ± 0.01	-29 ± 1	13.0 ± 1
Lip-PEG-HA	124 ± 4	0.12 ± 0.02	-34. ± 2	13.3 ± 1
Lip-HA	182 ± 9	0.19 ± 0.02	-38 ± 2	12.9 ± 0.5

3.2. DSC analysis

In addition to standard characterization by DLS, DSC analysis was carried out to measure the interaction between the HA-DPPE conjugates and the liposomes bilayers (Figure 1C). The DSC curve of pure DPPC showed a pre-transition peak at 37 °C indicative of the passage from the lamellar gel phase to the ripple gel phase. This temperature marks the beginning of the melting process when the flat DPPC bilayer shifts towards a periodically undulated conformation [39]. The primary transition temperature (Tm) was measured as 41.5 °C. This peak corresponds to the passage from a gel-ordered phase to a disordered lamellar liquid crystalline phase. At this temperature, phospholipids hydrocarbon chains change their intermolecular interactions and the space between each chain increases progressively until the establishment of a fluid disordered phase.

The addition of mPEG-DSPE induced an enlargement of the main phase transition peak without changing the main Tm (41.6 °C). On the other hand, adding the HA-DPPE conjugate induced a considerable flattening of the pre-transition peak, an enlargement and intensity reduction of the main transition peak, and an increase of the main transition temperature of 0.8 °C. As observed in the curve with HA, the peak broadening was associated with decreased lipid packing as previously reported [40]. This increase of the Tm suggests that the DPPE-HA is correctly inserted in the bilayers of the liposomes enabling cell HA-based cell targeting [41].

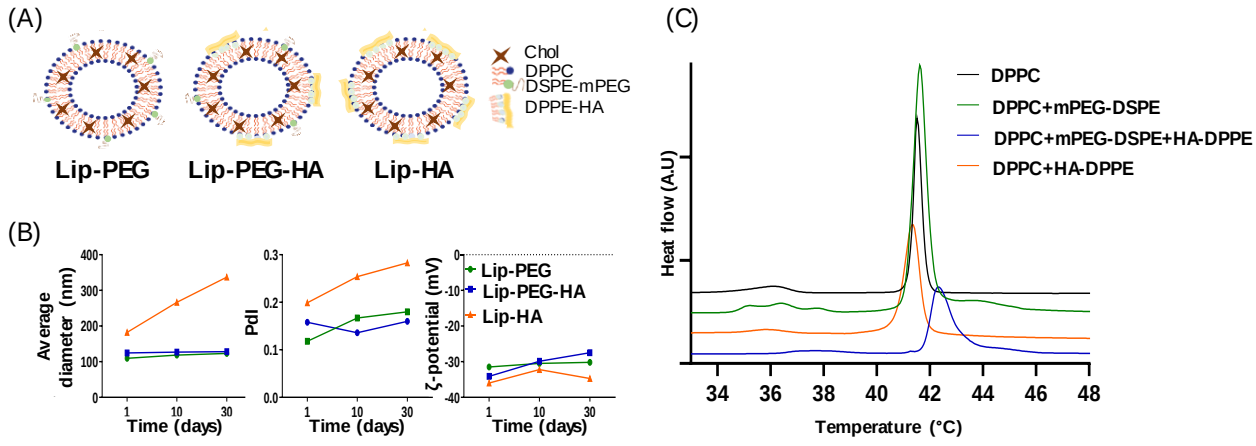

Figure 1: *Physical characteristics of the liposomal platforms. (A) Schematic structural differences of Lip-PEG, Lip-PEG-HA and Lip-HA; (B) Liposomes average diameter, PdI and ζ potential over 30 days after formulation; (C) DSC thermograms of liposomes composed of pure DPPC (black), DPPC+mPEG-*

DSPE (green), DPPC+mPEG-DSPE+HA-DPPE (blue) and DPPC+HA-DPPE (orange).

3.3. *In vitro* assays

3.3.1. Liposome uptake by inflammatory macrophages

The *in vitro* interactions of the three formulations with activated $CD44^{hi}$ M1 macrophages were measured by flow cytometry and compared to $CD44^{low}$ M0 macrophages (Figure 2A). M1 macrophage profile and subsequent CD44 increased expression [42] ($CD44^{hi}$) were confirmed by qPCR, flow cytometry and ELISA (Figures S1 and S2). Results displayed in Figure 2B reveal that untargeted Lip-PEG interact similarly with unstimulated M0 and M1 macrophages. However, the addition of HA moieties on the surface of the liposomes (Lip-PEG-HA and Lip-HA) led to a significantly higher uptake by $CD44^{hi}$ M1 macrophages compared to $CD44^{low}$ M0 macrophages. As expected, unstimulated M0 macrophages, which present a low but constitutive CD44 expression, also revealed a slight increase in interaction with Lip-PEG-HA and Lip-HA compared to Lip-PEG. Furthermore, M1 activated macrophages showed a higher interaction with Lip-HA than Lip-PEG-HA. This effect was expected as PEG has been shown to reduce cell receptor binding efficiency and cellular uptake [43–45].

Those distinctions in cellular uptake of the different liposome formulations, based on the presence of HA, were confirmed by fluorescence confocal microscopy. Captured images (Figure 2C) confirmed this trend with M1 cells incubated with Lip-HA revealing a higher liposome-associated red fluorescence signal than M1 cell treated with Lip-PEG or Lip-PEG-HA. However, confocal analysis of cells incubated with Lip-HA did not reveal a significant difference between M0 and M1. Additionally, close-up confocal images (Figures S3 and S4) revealed the presence of fluorescent signals inside the cells, indicative of cellular internalization.

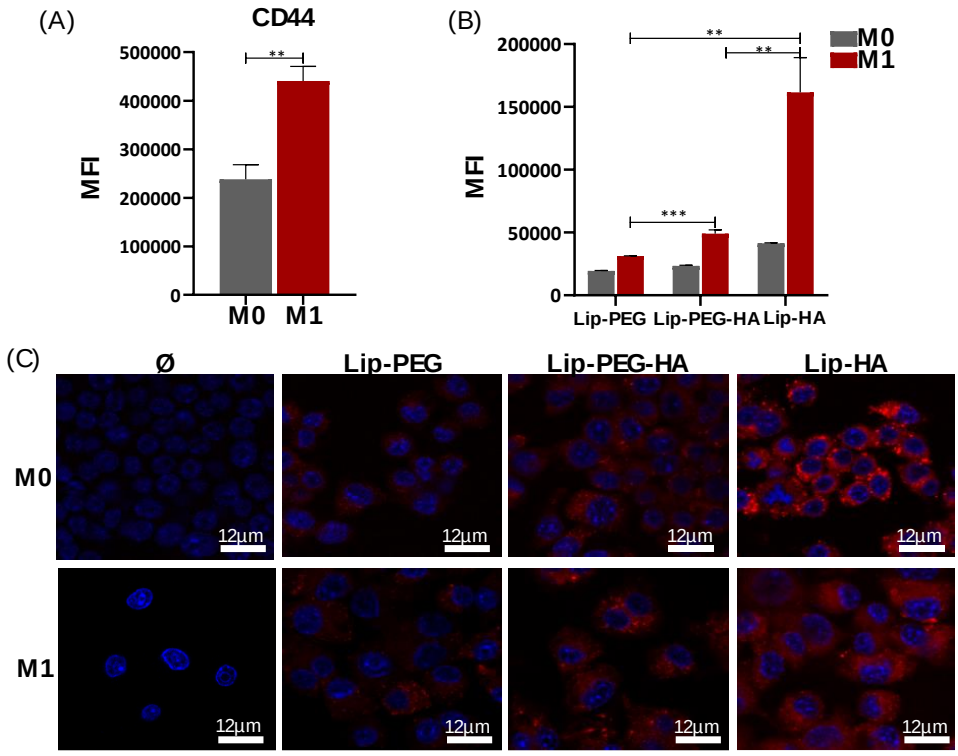

Figure 2: *In vitro analysis of liposomal platforms in polarized macrophages. (A) Effect on CD44 expression in M0 and M1 polarized RAW 264.7 cells, **p<0.01 (t-test); (B) Lip-PEG, Lip-PEG-HA and Lip-HA internalization in M0 and M1 cells after 6 hours of incubation. The statistical analysis refers to the comparison between Lip-PEG and Lip-PEG-HA; Lip-PEG and Lip-HA and Lip-PEG-HA and Lip-HA, ** p<0.01; *** p<0.001, in M1 cells (t-test); (C) Confocal images of RAW 264.7 M0 and M1 macrophages representing nuclei (blue) and liposomes (red). A greater Lip-HA internalization was observed for M0 and M1 cells. Scale bar, 12 µm. Data are presented as average ± SD of n=3 experiments.*

The internalization kinetics were studied over 24 h (Figure 3A). In M0 macrophages, the highest internalization rate occurred after 6 h, followed by a plateau. For M1 macrophages, the increase could be observed up to 24 h. The reduction in liposomes internalization rate as incubation times increased is suggestive of a saturation of the CD44 receptors [46]. It occurs primarily in M0 macrophages as they express less CD44 receptors than M1 macrophages. Thus, an incubation time of 6 h was kept for subsequent *in vivo* experiments.

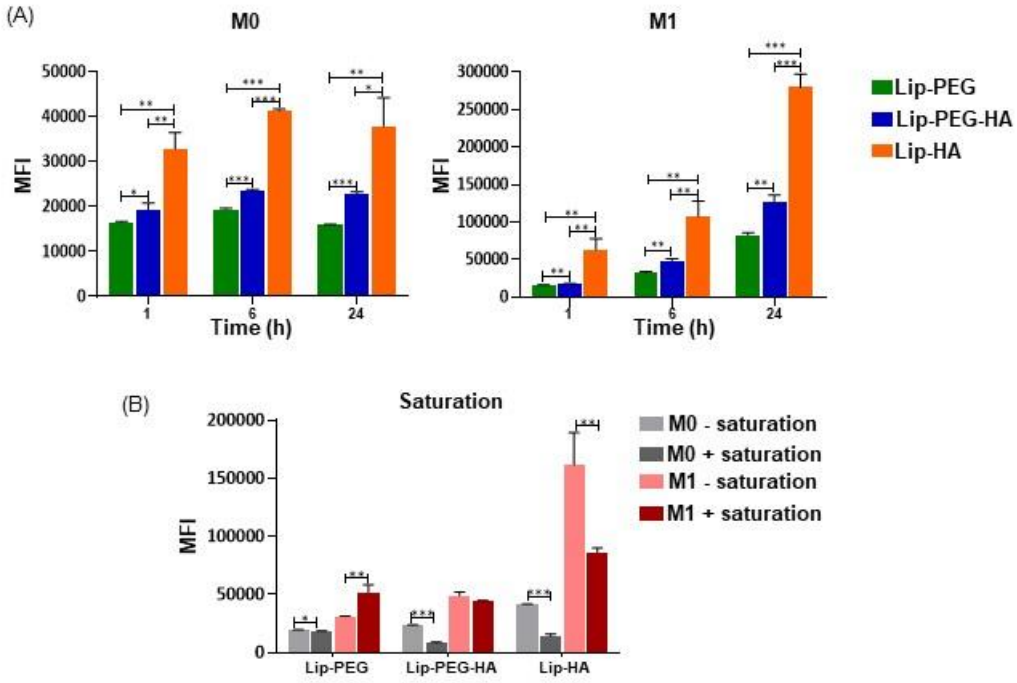

Figure 3: *In vitro liposomes internalization. (A) Internalization kinetics over 24 h of liposomal platforms in M0 and M1 macrophages; (B) Influence of CD44 saturation on liposomes internalization in M0 (grey) and M1 (pink) polarized macrophage cell. The statistical analysis refers to liposome internalization between cells where the CD44 receptors were saturated or not. Data are presented as average ± SD of n=3 experiments, where *p<0.05; **p<0.001 and ***p<0.0001.*

To confirm the influence of CD44 receptors on the uptake of liposomes, targeting experiments were carried out (Figure 3B) with cells pre-exposed to an excess of free hyaluronic acid (1 µM) to pre-saturate CD44 receptors [47]. As expected, CD44 saturation with free HA led to a reduction of $CD44^{hi}$ M1 macrophages interaction with Lip-HA indicative of the importance of CD44 receptors in the targeted uptake of HA-bearing liposomes. A similar pattern, although less pronounced was also observed in M0 macrophages. Again, this is most likely due to their lower CD44 expression. Unexpectedly, the addition of free HA before adding Lip-PEG revealed a non-anticipated small increase of macrophages interaction with PEGylated liposomes to a similar level to Lip-PEG-HA. We believe that this marginal experimental effect could be caused by electrostatic interactions between the PEGylated liposomes and the free HA

present in the solution or bound to CD44 [37]. However, this did not occur with Lip-PEG-HA as PEG chains hinder the presence of HA on particle surface, reducing binding interaction with CD44 receptor as previously shown for folic-acid liposomes upon binding folate receptor [45].

All together these *in vitro* results demonstrate that HA conjugation on the surface of the liposomes is critical to induce a CD44-associated M1 macrophages active targeting while addition of PEG molecules tend to reduce the efficacy of this CD44 targeting.

3.3.2. Mucopenetrating properties

As described earlier, the ability of nanoparticles to cross the mucus layer is critical to achieve efficient drug delivery in the lungs [14] with PEGylation of the particle surface being one of the best strategy [17]. In our study, the diffusion movements in mucus of fluorescein labelled Lip-PEG, Lip-PEG-HA and Lip-HA were evaluated by multiple tracking analyses [38]. All the liposomal formulations showed Brownian-like particle trajectories (Figure 4A) indicative of possible passage through the mucin solution. Surprisingly, Lip-PEG-HA liposomes displayed the highest MSD, followed by Lip-HA and Lip-PEG (Figure 4B). Those results could be caused by the HA coating that reduces mucin adsorption while its hydrophilicity increases the diffusion of nanoparticles through the mucus mesh [48]. This reduced mucin adsorption may be explained by the repulsive forces caused by polyanionic domains of HA and mucin chains and may be the driving force that increases permeability through the mucus layer.

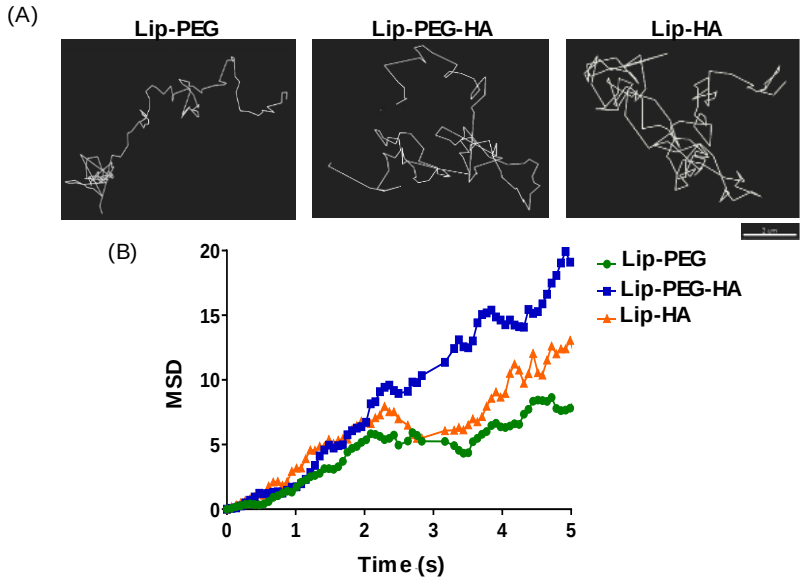

Figure 4: *Lip-PEG; Lip-PEG-HA and Lip-HA diffusion in mucin solution. (A) Representative trajectories of liposomes. Scale bar, 2 µm. (B) MSD of liposomes as a function of the time.*

3.4. *In vivo* studies

Macrophages are the first immune cells that encounter incoming pathogens in the lungs [49]. They play an important role in the initiation and resolution of the immune response [50]. To evaluate the behavior of the three liposome platforms in an inflammatory condition *in vivo*, we established a LPS-based lung inflammatory model in C57BL/6J mice [51]. Flow cytometry analyses of the BALF 24 h after LPS exposure show an increase in numbers of neutrophils and macrophages (Figure S4). Additional analyses revealed an increase in cellular expressions of pro-inflammatory markers such as iNOS, CD86 and CD44 in cell BALF cells extracted from mice treated with LPS, compared to control mice treated with PBS, confirming a change in macrophage phenotype and the increase proportion of M1-macrophages in BALF after LPS challenge (Figure S5).

The cellular uptake of different liposomes in BALF and lung cells were then assessed. 24 h after exposure to LPS, Rhodamine-labeled Lip-PEG, Lip-PEG-HA or Lip-HA were instilled into the mice lungs at a fixed rhodamine dose. 6 h after instillation, the animals were sacrificed and BALF and lung tissues were extracted, processed, and analyzed by flow cytometry to quantify the liposomal uptake by different cellular populations (Figure 5A). Interestingly flow cytometry

data revealed that all liposomes were taken up at a similar proportion by BALF macrophages. However, when focusing on Siglec F^{hi} alveolar macrophages, the measures revealed a substantial heterogeneity between animals. While several animals showed no targeting of this population, another reveals a strong (>10%) targeting. This may be explained by the propensity of the Lip-HA particles to aggregate and concentrate themselves in either macrophage poor or rich sections of the alveoli. Surprisingly, neutrophils in BALF demonstrated a notable preferential interaction with Lip-PEG (Figure 5B) compared to the other liposomes. This neutrophil targeting was not expected but may be very useful for future studies as neutrophils are known to be key cellular targets in many inflammatory lung diseases associated with acute respiratory distress syndrome such as COVID-19 [52,53].

When studying cells extracted from the lungs (Figure 5C), those showed an expected lower liposomal uptake ratio than their BALF counterparts. Interestingly this pattern is particularly marked for macrophages. Comparison between the different liposomes and cell populations showed that Lip-PEG-HA formulations were not as effective as expected in penetrating the mucus and interacting with lung macrophages. Neutrophils in the lung tissue present a similar pattern as for the BALF, revealing a possible better uptake of Lip-HA by alveolar macrophages and a higher neutrophil targeting by Lip-PEG. Those results show that surface alteration of liposomes may induce alteration in cell distribution and the possibility of selecting the most suitable liposome platform formulation depending on the tissue or targeted cells.

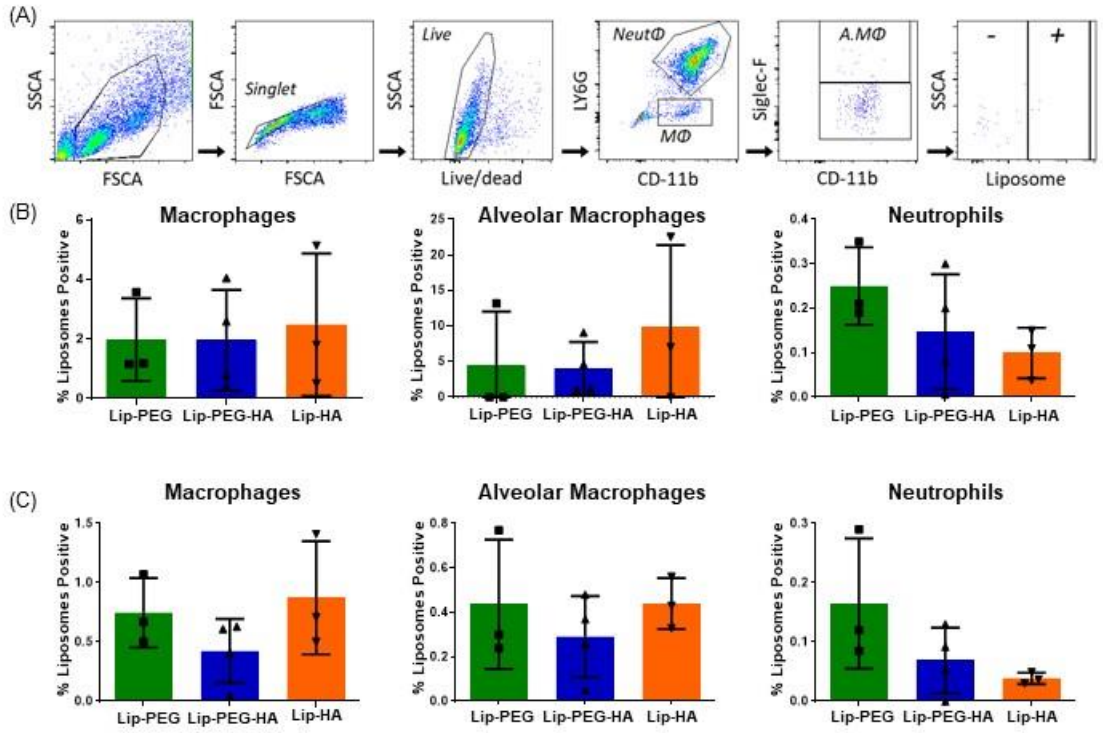

Figure 5: *In vivo liposomes internalization in LPS treated mice. (A) Gating strategy used to quantify liposomes into macrophages, alveolar macrophages or neutrophils in the LPS treated mice. Cells were isolated from enzymatically digested mouse lungs, and after debris and doublets exclusion, live cells were selected using live/dead staining. A minimal panel of surface markers was used to identify Macrophages (MΦ: CD11b^{+} Ly6G^{-}) from Neutrophils (NeutΦ: CD11^{+} Ly6G^{+}); after macrophages selection, Alveolar Macrophages (A. MΦ: SiglecF^{+}) were identified. Macrophage, alveolar macrophage and neutrophils internalization of Lip-PEG, Lip-PEG-HA and Lip-HA was quantified in (B) BALF and (C) lungs by flow cytometry (n=3).*

Conclusions

This study investigated the production of three different liposomes by the one-step ethanol injection method as a strategy to improve specificity in the treatment of lung diseases. A model of inflammatory macrophage (M1) was developed *in vitro,* and its characterization showed an increase in CD44 receptors when compared to unstimulated macrophages. These receptors are formed by a type I transmembrane glycoprotein that binds to hyaluronic acid (HA) in most cell types. Despite the proven mucopenetrating ability of PEG, *in vitro* experiments showed a higher rate of internalization for Lip-HA when

compared to the other two platforms that contained PEG. The same behaviour was observed *in vivo* in BALF alveolar macrophages as they presented a lower internalization rate for liposomes with PEG in their composition unlike neutrophils. This shows the high efficiency of Lip-HA in recognizing CD44 receptors. These results show a balance between mucus penetration and receptor targeting. Therefore, the site of action and the targeted cells must be considered when choosing the most appropriate platform for the treatment of lung diseases.

Author Contributions

K.B.J, F.F, N.T and E.F. conceptualized and designed the study. K.B.J., A.M., C.C., Y.L., S.D. and D.C conducted the experiments. F.F. and E.F supervised the research. K.B.J and T.L.N performed statistical analysis. K.B.J, FF, T.L.N., N.T., E.M.L. and E.F. analyzed the data and wrote the manuscript. All authors discussed the progress of research and reviewed the manuscript.

Conflicts of interest

The authors declare no conflicts of interest.

Acknowledgements

KBJ acknowledges a scholarship from Programa de Pós-Graduação em Nanotecnologia Farmacêutica of Federal University of Goiás/CAPES, a CAPES scholarship from the Doctoral Program Abroad (Process n. 88881.361526/2019-01), also a scholarship from the doctoral school: ED Innovation Thérapeutique – Du Fondamental à l'Appliqué [ITFA n. 569], and Institut Galien Paris-Saclay (UMR 8612) of University Paris-Saclay. AM post-doctoral fellowship was funded by EuroNanomed III (ARROWNANO 2017-1892). The authors acknowledge Claudine Delomenie and ACTAGen, Valérie Domergue and AnimEx, and Valérie Nicolas and MIPSIT, all core facilities from IPSIT, for access to their equipment/ infrastructures and advice. We also thank the Région Ile-de-France for financial support of the IPSIT platforms.

Formatting of funding sources

This work was funded by Brazilian agency Coordenação de Aperfeiçoamento de Pessoal de Nível Superior (CAPES) and French agency Centre National de la Recherche Scientifique (CNRS UMR 8612). Authors acknowledge financial support from ANR (ANR JCJC NANOSEPSIS FF). FF is a member of the FHU SEPSIS (Saclay and Paris Seine Nord Endeavour to PerSonalize Interventions for Sepsis).

Notes and references

[1] E. Mitsi, R. Kamng'ona, J. Rylance, C. Solórzano, J. Jesus Reiné, H.C. Mwandumba, D.M. Ferreira, K.C. Jambo, Human alveolar macrophages predominately express combined classical M1 and M2 surface markers in steady state, Respir. Res. 19 (2018) 1–4. https://doi.org/10.1186/s12931-018-0777-0.

[2] D. Wang, N. Phan, C. Isely, L. Bruene, K.M. Bratlie, Effect of surface modification and macrophage phenotype on particle internalization, Biomacromolecules. 15 (2014) 4102–4110. https://doi.org/10.1021/bm5011382.

[3] L.P. Nicod, Lung defences: An overview, Eur. Respir. Rev. 14 (2005) 45–50. https://doi.org/10.1183/09059180.05.00009501.

[4] J.K.W. Lam, W. Liang, H.K. Chan, Pulmonary delivery of therapeutic siRNA, Adv. Drug Deliv. Rev. 64 (2012) 1–15. https://doi.org/10.1016/j.addr.2011.02.006.

[5] L.E. Ostrowski, W.D. Bennett, Cilia and Mucociliary Clearance, Encycl. Respir. Med. Four-Volume Set. (2006) 466–470. https://doi.org/10.1016/B0-12-370879-6/00079-X.

[6] L. Wang, Y. Zhang, N. Zhang, J. Xia, Q. Zhan, C. Wang, Potential role of M2 macrophage polarization in ventilator-induced lung fibrosis, Int. Immunopharmacol. 75 (2019) 105795–105795. https://doi.org/10.1016/j.intimp.2019.105795.

[7] E. Bazzan, G. Turato, M. Tinè, C.M. Radu, E. Balestro, C. Rigobello, D. Biondini, M. Schiavon, F. Lunardi, S. Baraldo, F. Rea, P. Simioni, F. Calabrese, M. Saetta, M.G. Cosio, Dual polarization of human alveolar macrophages progressively increases with smoking and COPD severity, Respir. Res. 18 (2017) 1–8. https://doi.org/10.1186/s12931-017-0522-0.

[8] P. Muralidharan, M. Malapit, E. Mallory, D. Hayes, H.M. Mansour, Inhalable nanoparticulate powders for respiratory delivery, Nanomedicine Nanotechnology, Biol. Med. 11 (2015) 1189–1199. https://doi.org/10.1016/j.nano.2015.01.007.

[9] C. Yunna, H. Mengru, W. Lei, C. Weidong, Macrophage M1/M2 polarization, Eur. J. Pharmacol. 877 (2020). https://doi.org/10.1016/j.ejphar.2020.173090.

[10] P.P. Mehta, D. Ghoshal, A.P. Pawar, S.S. Kadam, V.S. Dhapte-Pawar, Recent advances in inhalable liposomes for treatment of pulmonary diseases: Concept to clinical stance, J. Drug Deliv. Sci. Technol. 56 (2020) 101509. https://doi.org/10.1016/j.jddst.2020.101509.

[11] R. Vlahos, S. Bozinovski, Role of Alveolar Macrophages in Chronic Obstructive Pulmonary Disease, Front. Immunol. 5 (2014). https://doi.org/10.3389/FIMMU.2014.00435.

[12] W.H. Lee, C.Y. Loo, D. Traini, P.M. Young, Inhalation of nanoparticle-based drug for lung cancer treatment: Advantages and challenges, Asian J. Pharm. Sci. 10 (2015) 481–489. https://doi.org/10.1016/j.ajps.2015.08.009.

[13] M. Ghadiri, P.M. Young, D. Traini, Strategies to enhance drug absorption via nasal and pulmonary routes, Pharmaceutics. 11 (2019). https://doi.org/10.3390/pharmaceutics11030113.

[14] I. Roy, N. Vij, Nanodelivery in airway diseases: Challenges and therapeutic applications, Nanomedicine Nanotechnology, Biol. Med. 6 (2010) 237–244. https://doi.org/10.1016/j.nano.2009.07.001.

[15] H.M. Mansour, Y.S. Rhee, X. Wu, Nanomedicine in pulmonary delivery., Int. J. Nanomedicine. 4 (2009) 299–319. https://doi.org/10.2147/ijn.s4937.

[16] J.T. Huckaby, S.K. Lai, PEGylation for enhancing nanoparticle diffusion in mucus, Adv. Drug Deliv. Rev. 124 (2018) 125–139. https://doi.org/10.1016/j.addr.2017.08.010.

[17] G. Osman, J. Rodriguez, S.Y. Chan, J. Chisholm, G. Duncan, N. Kim, A.L. Tatler, K.M. Shakesheff, J. Hanes, J.S. Suk, J.E. Dixon, PEGylated enhanced cell penetrating peptide nanoparticles for lung gene therapy, J. Control. Release. 285 (2018) 35–45. https://doi.org/10.1016/j.jconrel.2018.07.001.

[18] J.G. Weers, J. Bell, H.K. Chan, D. Cipolla, C. Dunbar, A.J. Hickey, I.J. Smith, Pulmonary formulations: What remains to be done?, J. Aerosol Med. Pulm. Drug Deliv. 23 (2010). https://doi.org/10.1089/jamp.2010.0838.

[19] A. Costa, B. Sarmento, V. Seabra, Targeted Drug Delivery Systems for Lung Macrophages, Curr. Drug Targets. 16 (2014) 1565–1581. https://doi.org/10.2174/1389450115666141114152713.

[20] J. Yoo, C. Park, G. Yi, D. Lee, H. Koo, Active Targeting Strategies Using Biological Ligands for Nanoparticle Drug Delivery Systems, Cancers (Basel). 11 (2019). https://doi.org/10.3390/CANCERS11050640.

[21] N. TL, H. H, V. J, F. E, Lipid-based nanosystems for CD44 targeting in cancer treatment: recent significant advances, ongoing challenges and unmet needs, Nanomedicine (Lond). 11 (2016) 1865–1887. https://doi.org/10.2217/NNM-2016-5000.

[22] A.P.B. Almeida, G.B.R. Damaceno, A.F. Carneiro, A. Bohr, H.R. Gonçalves, M.C. Valadares, T.L. Nascimento, E.M. Lima, Mucopenetrating lipoplexes modified with PEG and hyaluronic acid for CD44-targeted local siRNA delivery to the lungs, J. Biomater. Appl. 34 (2019) 617–630. https://doi.org/10.1177/0885328219863291.

[23] W. Alshaer, H. Hillaireau, J. Vergnaud, S. Ismail, E. Fattal, Functionalizing Liposomes with anti-CD44 Aptamer for Selective Targeting of Cancer Cells, Bioconjug. Chem. 26 (2015) 1307–1313. https://doi.org/10.1021/bc5004313.

[24] L. Arabi, A. Badiee, F. Mosaffa, M.R. Jaafari, Targeting CD44 expressing cancer cells with anti-CD44 monoclonal antibody improves cellular uptake and antitumor efficacy of liposomal doxorubicin, J. Control. Release. 220 (2015) 275–286. https://doi.org/10.1016/j.jconrel.2015.10.044.

[25] S. Arpicco, C. Lerda, E. Dalla Pozza, C. Costanzo, N. Tsapis, B. Stella, M. Donadelli, I. Dando, E. Fattal, L. Cattel, M. Palmieri, Hyaluronic acid-coated liposomes for active targeting of gemcitabine, Eur. J. Pharm. Biopharm. 85 (2013) 373–380. https://doi.org/10.1016/j.ejpb.2013.06.003.

[26] M. KM, K. E, A. AV, B. RV, Masking and triggered unmasking of targeting ligands on nanocarriers to improve drug delivery to brain tumors, Biomaterials. 30 (2009) 3986–3995. https://doi.org/10.1016/J.BIOMATERIALS.2009.04.012.

[27] Z. Shen, A. Fisher, W.K. Liu, Y. Li, PEGylated “stealth” nanoparticles and liposomes, Eng. Biomater. Drug Deliv. Syst. Beyond Polyethyl. Glycol. (2018) 1–26. https://doi.org/10.1016/B978-0-08-101750-0.00001-5.

[28] L. Pandolfi, A. Marengo, K.B. Japiassu, V. Frangipane, N. Tsapis, V. Bincoletto, V. Codullo, S. Bozzini, M. Morosini, S. Lettieri, V. Vertui, D. Piloni,

S. Arpicco, E. Fattal, F. Meloni, Liposomes Loaded with Everolimus and Coated with Hyaluronic Acid: A Promising Approach for Lung Fibrosis, Int. J. Mol. Sci. 2021, Vol. 22, Page 7743. 22 (2021) 7743. https://doi.org/10.3390/IJMS22147743.

[29] C. Jaafar-Maalej, R. Diab, V. Andrieu, A. Elaissari, H. Fessi, Ethanol injection method for hydrophilic and lipophilic drug-loaded liposome preparation, J. Liposome Res. 20 (2010) 228–243. https://doi.org/10.3109/08982100903347923.

[30] S. Knapp, S. Florquin, D.T. Golenbock, LPS-Induced Lung Inflammation In Vivo (LPS)-Binding Protein Inhibits the Pulmonary Lipopolysaccharide Tom van der Poll, (2021). https://doi.org/10.4049/jimmunol.176.5.3189.

[31] L. Aragao-Santiago, H. Hillaireau, N. Grabowski, S. Mura, T.L. Nascimento, S. Dufort, J.-L. Coll, N. Tsapis, E. Fattal, Compared in vivo toxicity in mice of lung delivered biodegradable and non-biodegradable nanoparticles, Nanotoxicology. 10 (2016) 292–302. https://doi.org/10.3109/17435390.2015.1054908.

[32] M.S. Braza, M.M.T. van Leent, M. Lameijer, B.L. Sanchez-Gaytan, R.J.W. Arts, C. Pérez-Medina, P. Conde, M.R. Garcia, M. Gonzalez-Perez, M. Brahmachary, F. Fay, E. Kluza, S. Kossatz, R.J. Dress, F. Salem, A. Rialdi, T. Reiner, P. Boros, G.J. Strijkers, C.C. Calcagno, F. Ginhoux, I. Marazzi, E. Lutgens, G.A.F. Nicolaes, C. Weber, F.K. Swirski, M. Nahrendorf, E.A. Fisher, R. Duivenvoorden, Z.A. Fayad, M.G. Netea, W.J.M. Mulder, J. Ochando, Inhibiting Inflammation with Myeloid Cell-Specific Nanobiologics Promotes Organ Transplant Acceptance, Immunity. 49 (2018) 819-828.e6. https://doi.org/10.1016/j.immuni.2018.09.008.

[33] D. Cosco, N. Tsapis, T.L. Nascimento, M. Fresta, D. Chapron, M. Taverna, S. Arpicco, E. Fattal, Polysaccharide-coated liposomes by post-insertion of a hyaluronan-lipid conjugate, Colloids Surfaces B Biointerfaces. 158 (2017) 119–126. https://doi.org/10.1016/j.colsurfb.2017.06.029.

[34] T.L. Nascimento, H. Hillaireau, J. Vergnaud, E. Fattal, Lipid-based nanosystems for CD44 targeting in cancer treatment: recent significant advances, ongoing challenges and unmet needs., Nanomedicine (Lond). 11 (2016) 1865–87. https://doi.org/10.2217/nnm-2016-5000.

[35] S. Arpicco, M. Bartkowski, A. Barge, D. Zonari, L. Serpe, P. Milla, F. Dosio, B.

Stella, S. Giordani, Effects of the Molecular Weight of Hyaluronic Acid in a Carbon Nanotube Drug Delivery Conjugate, Front. Chem. 8 (2020) 1–12. https://doi.org/10.3389/fchem.2020.578008.

[36] L. Pandolfi, V. Frangipane, C. Bocca, A. Marengo, E.T. Genta, S. Bozzini, M. Morosini, M. D'Amato, S. Vitulo, M. Monti, G. Comolli, M.T. Scupoli, E. Fattal, S. Arpicco, F. Meloni, Hyaluronic acid-decorated liposomes as innovative targeted delivery system for lung fibrotic cells, Molecules. 24 (2019) 3291. https://doi.org/10.3390/molecules24183291.

[37] Y. Tiantian, Z. Wenji, S. Mingshuang, Y. Rui, S. Shuangshuang, M. Yuling, Y. Jianhua, Y. Xinggang, W. Shujun, P. Weisan, Study on intralymphatic-targeted hyaluronic acid-modified nanoliposome: Influence of formulation factors on the lymphatic targeting, Int. J. Pharm. 471 (2014) 245–257. https://doi.org/10.1016/j.ijpharm.2014.05.027.

[38] M. Boegh, H.M. Nielsen, Mucus as a barrier to drug delivery - Understanding and mimicking the barrier properties, Basic Clin. Pharmacol. Toxicol. 116 (2015) 179–186. https://doi.org/10.1111/bcpt.12342.

[39] J.R. Banigan, A. Gayen, N.J. Traaseth, Correlating lipid bilayer fluidity with sensitivity and resolution of polytopic membrane protein spectra by solid-state NMR spectroscopy, Biochim. Biophys. Acta - Biomembr. 1848 (2015) 334–341. https://doi.org/10.1016/j.bbamem.2014.05.003.

[40] D.A. Mannock, R.N.A.H. Lewis, R.N. McElhaney, Comparative Calorimetric and Spectroscopic Studies of the Effects of Lanosterol and Cholesterol on the Thermotropic Phase Behavior and Organization of Dipalmitoylphosphatidylcholine Bilayer Membranes, Biophys. J. 91 (2006) 3327–3340. https://doi.org/10.1529/BIOPHYSJ.106.084368.

[41] M.I. Morandi, M. Sommer, M. Kluzek, F. Thalmann, A.P. Schroder, C.M. Marques, DPPC Bilayers in Solutions of High Sucrose Content, Biophys. J. 114 (2018) 2165–2173. https://doi.org/10.1016/j.bpj.2018.04.003.

[42] J.M. Rios de la Rosa, A. Tirella, A. Gennari, I.J. Stratford, N. Tirelli, The CD44-Mediated Uptake of Hyaluronic Acid-Based Carriers in Macrophages, Adv. Healthc. Mater. 6 (2017) 1–11. https://doi.org/10.1002/adhm.201601012.

[43] H. Hatakeyama, H. Akita, H. Harashima, The Polyethyleneglycol Dilemma: Advantage and Disadvantage of PEGylation of Liposomes for Systemic Genes and Nucleic Acids Delivery to Tumors, Biol. Pharm. Bull. 36 (2013) 892–899.

https://doi.org/10.1248/BPB.B13-00059.

[44] D. Pozzi, V. Colapicchioni, G. Caracciolo, S. Piovesana, A.L. Capriotti, S. Palchetti, S. De Grossi, A. Riccioli, H. Amenitsch, A. Laganà, Effect of polyethyleneglycol (PEG) chain length on the bio–nano-interactions between PEGylated lipid nanoparticles and biological fluids: from nanostructure to uptake in cancer cells, Nanoscale. 6 (2014) 2782–2792. https://doi.org/10.1039/C3NR05559K.

[45] A. Gabizon, A.T. Horowitz, D. Goren, D. Tzemach, F. Mandelbaum-Shavit, M.M. Qazen, S. Zalipsky, Targeting Folate Receptor with Folate Linked to Extremities of Poly(ethylene glycol)-Grafted Liposomes: In Vitro Studies, Bioconjug. Chem. 10 (1999) 289–298. https://doi.org/10.1021/BC9801124.

[46] M. Takeda, H. Terasawa, M. Sakakura, Y. Yamaguchi, M. Kajiwara, H. Kawashima, M. Miyasaka, I. Shimada, Hyaluronan Recognition Mode of CD44 Revealed by Cross-saturation and Chemical Shift Perturbation Experiments, J. Biol. Chem. 278 (2003) 43550–43555. https://doi.org/10.1074/jbc.M308199200.

[47] M.M. Knüpfer, H. Poppenborg, M. Hotfilder, K. Kühnel, J.E.A. Wolff, M. Domula, CD44 expression and hyaluronic acid binding of malignant glioma cells, Clin. Exp. Metastasis. 17 (1999) 71–76. https://doi.org/10.1023/A:1026425519497.

[48] L. Liu, C. Tian, B. Dong, M. Xia, Y. Cai, R. Hu, Models to evaluate the barrier properties of mucus during drug diffusion, 599 (2021).

[49] A.C. Kirby, M.C. Coles, P.M. Kaye, Alveolar Macrophages Transport Pathogens to Lung Draining Lymph Nodes, J. Immunol. 183 (2009) 1983–1989. https://doi.org/10.4049/jimmunol.0901089.

[50] G. Hu, J.W. Christman, Editorial: Alveolar macrophages in lung inflammation and resolution, Front. Immunol. 10 (2019) 2275. https://doi.org/10.3389/fimmu.2019.02275.

[51] B. Beutler, E.T. Rietschel, Innate immune sensing and its roots: The story of endotoxin, Nat. Rev. Immunol. 3 (2003) 169–176. https://doi.org/10.1038/nri1004.

[52] Y. Su, J. Gao, P. Kaur, Z. Wang, Neutrophils and Macrophages as Targets for Development of Nanotherapeutics in Inflammatory Diseases, Pharmaceutics. 12 (2020) 1–24. https://doi.org/10.3390/PHARMACEUTICS12121222.

[53] F. Montenegro, L. Unigarro, G. Paredes, T. Moya, A. Romero, L. Torres, J.C. López, F.E.J. González, G. Del Pozo, A. López-Cortés, A.M. Diaz, E. Vasconez, D. Cevallos-Robalino, A. Lister, E. Ortiz-Prado, Acute respiratory distress syndrome (ARDS) caused by the novel coronavirus disease (COVID-19): a practical comprehensive literature review, Expert Rev. Respir. Med. 15 (2021) 183–195. https://doi.org/10.1080/17476348.2020.1820329.